Available online at www.sciencedirect.com
SCIENCE DIRECT®
Earth and Planetary Science Letters 222 (2004) 259–273
EPSL
www.elsevier.com/locate/epsl

Tracing the history of submarine hydrothermal inputs and the significance of hydrothermal hafnium for the seawater budget—a combined Pb–Hf–Nd isotope approach

Tina van de Flierdt[a,b,*], Martin Frank[b], Alex N. Halliday[b], James R. Hein[c], Bodo Hattendorf[d], Detlef Günther[d], Peter W. Kubik[e]

[a] *Lamont-Doherty Earth Observatory of Columbia University, 61 Route 9W, Palisades, NY 10964, USA*
[b] *Institute for Isotope Geology and Mineral Resources, Department of Earth Sciences, ETH-Zentrum, Sonneggstrasse 5, CH- 8092 Zürich, Switzerland*
[c] *U.S. Geological Survey, 345 Middlefield Road, MS-999, Menlo Park, CA 94025, USA*
[d] *Laboratory of Inorganic Chemistry, Department of Chemistry, ETH Hönggerberg, Wolfgang-Pauli-Strasse 10, CH-8093 Zürich, Switzerland*
[e] *Paul Scherrer Institute, c/o Institute for Particle Physics, ETH Hönggerberg, CH-8093 Zürich, Switzerland*

Received 2 September 2003; received in revised form 9 February 2004; accepted 18 February 2004

Abstract

Secular variations in the Pb isotopic composition of a mixed hydrogenous-hydrothermal ferromanganese crust from the Bauer Basin in the eastern Equatorial Pacific provide clear evidence for changes in hydrothermal contributions during the past 7 Myr. The nearby Galapagos Rise spreading center provided a strong hydrothermal flux prior to 6.5 Ma. After 6.5 Ma, the Pb became stepwise more radiogenic and more similar to Equatorial Pacific seawater, reflecting the westward shift of spreading to the presently active East Pacific Rise (EPR). A second, previously unrecognized enhanced hydrothermal period occurred between 4.4 and 2.9 Ma, which reflects either off-axis hydrothermal activity in the Bauer Basin or a late-stage pulse of hydrothermal Pb from the then active, but waning Galapagos Rise spreading center.

Hafnium isotope time-series of the same mixed hydrogenous-hydrothermal crust show invariant values over the past 7 Myr. Hafnium isotope ratios, as well as Nd isotope ratios obtained for this crust, are identical to that of hydrogenous Equatorial Pacific deep water crusts and clearly indicate that hydrothermal Hf, similar to Nd, does not travel far from submarine vents. Therefore, we suggest that hydrothermal Hf fluxes do not contribute significantly to the global marine Hf budget.

Keywords: hydrothermal fluids; Hf isotopes; Pb isotopes; ferromanganese crusts; Galapagos Rise

1. Introduction

Submarine hydrothermal vent fluids typically exhibit compositions distinct from that of seawater for a large range of elements (e.g. [1–4]). When vent fluids mix with ambient seawater, a significant frac-

* Corresponding author. Now at: Lamont-Doherty Earth Observatory of Columbia University, 61 Route 9W, Palisades, NY 10964, USA. Tel.: +1-845-365-8606; fax: +1-845-365-8155.
E-mail address: tina@ldeo.columbia.edu (T. van de Flierdt).

0012-821X/$ - see front matter © 2004 Elsevier B.V. All rights reserved.
doi:10.1016/j.epsl.2004.02.025

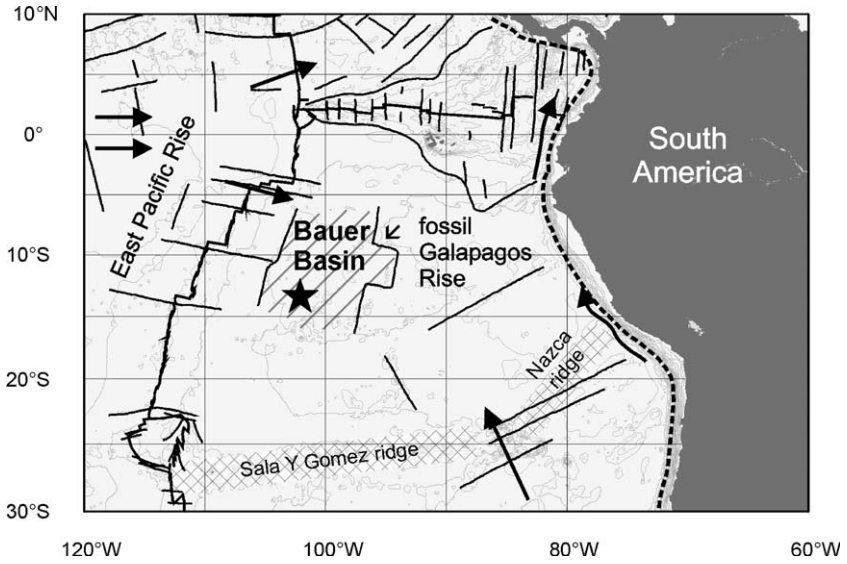

Fig. 1. Map of the eastern Equatorial Pacific, showing spreading centers of the East Pacific Rise (thick black lines), transform faults (thin black lines), subduction zones (dashed lines) and the recovery site of crust Yaloc (black star). The hatched area marks the Bauer Basin, which is bordered to the east by the fossil Galapagos Rise and to the west by the Bauer Scarp. Black arrows mark schematically the deep water circulation after Lonsdale [46].

tion of the dissolved metals precipitate instantaneously as sulfides (e.g. Fe and Pb; [5]). Other hydrothermal particles, mainly Fe oxyhydroxides, are transported within the hydrothermal plume and Mn oxyhydroxides are transported even farther. Hydrothermal plumes develop due to the buoyancy of hydrothermal fluids emerging from a vent and are subsequently dispersed by ocean currents (e.g. [6,7]). Such dispersion can extend up to 2000 km from the ridge crest as shown by ^{3}He anomalies west of the East Pacific Rise (EPR) [8]. Hydrothermal vent fields are, however, dynamic, commonly relatively short-lived, and venting waxes and wanes at any one site over time [9–11].

The locations of presently active segments of mid-ocean ridges and associated hydrothermal plumes can be identified by a range of geochemical tools such as the core top distribution of the Al/(Al + Fe + Mn) ratio

Table 1
Be concentrations and age model for crust Yaloc (D22-3)

Depth interval [mm]	^{10}Be [atoms/g]$*10^{-8}$ $\pm 1\sigma$ S.E.	^{9}Be$_{measured}$ [ppm]	^{9}Be$_{corrected}$ [ppm]	^{10}Be/^{9}Be $*10^{-8}$ $\pm 1\sigma$ S.E.	Growth rate [mm/Myr]
0–1.0	191.9 ± 9.5	1.3	2.4	12.15 ± 2.51	4.6
1.5–2.5	302.3 ± 8.5	2.3	4.0	11.35 ± 2.29	4.6
5.5–6.5	220.5 ± 9.3	2.7	4.8	6.93 ± 1.42	4.6
9.5–10.5	176.8 ± 7.3	3.2	5.6	4.74 ± 0.97	4.6
15–16	98.7 ± 4.9	2.6	4.6	3.19 ± 0.66	8.6
19.5–20.5	110.7 ± 4.4	2.9	5.1	3.28 ± 0.67	8.6
24–25	84.33 ± 4.12	2.7	4.9	2.60 ± 0.54	8.6
28.5–29.5	68.43 ± 7.33	3.0	5.3	1.92 ± 0.44	8.6
35–36	53.32 ± 4.89	3.7	6.5	1.22 ± 0.27	8.6
61–62	30.96 ± 2.00	4.6	8.1	0.58 ± 0.12	15.8

Measured Be concentration data correspond to the original ICP-MS analysis. The corrected data are normalized to the ratio between the measured values in Nod A-1 and the Nod A-1 values published by Axelsson et al. [63].

from metalliferous sediments [12]. These metalliferous sediments are anomalously enriched in transition metals relative to Al and other rock-forming elements since they incorporate significant amounts of particles derived from hydrothermal plumes (up to 94%; [13]). One alternative tool to determine the proportions of hydrothermal material in metalliferous sediments is their Pb isotopic composition (e.g. [6,14–20]). Lead shows a mid-ocean ridge basalt (MORB)-like isotopic composition in hydrothermal vent fluids, which is very different from that of ambient seawater (e.g. [21]). Furthermore, Pb has a relatively short residence time in deep waters (50–200 years; [22–24]) that makes Pb isotopes an excellent recorder for local hydrothermal inputs (e.g. [25]). Lead isotopes in surface sediments of the Bauer Basin (eastern Equatorial Pacific) indicate a decreasing proportion of hydrothermal material with increasing distance from the East Pacific Rise and at the same time an enhanced overprinting by hydrogenous (seawater-derived) Pb [14–16,18]. Although some cases have been reported, in which also Nd isotopes in metalliferous sediments [6] or ferromanganese crusts [26] show a mantle-derived origin, the isotopic composition of Nd in metalliferous sediments from near the East Pacific Rise is generally completely unaffected by hydrothermal contributions. This decoupling is caused by increased particulate concentrations in or near vents resulting in very efficient scavenging and a Nd residence time near hydrothermal vents of <1 year [27,28].

Provided that other potential contributors of Pb at a particular location, such as terrigenous particles, have remained near constant, which can be ascertained in part from the Nd isotopic composition, it should be possible to estimate the relative contribution of hydrothermally supplied Pb with time as a function of tectonic processes from mixed hydrogenous-hydrothermal ferromanganese crusts. By comparison with the inferred hydrothermal Pb contributions, it should moreover be possible to achieve some robust constraints on the significance of hydrothermal Hf contributions to the seawater budget of dissolved Hf, which has been subject of debate (e.g. [29,30]). This is the first case study that applies the combined Pb–Nd–Hf isotope evolution of a mixed hydrogenous-hydrothermal ferromanganese crust from near the Galapagos Rise in the eastern Equatorial Pacific for this purpose. Compared with metalliferous sediments, ferromanganese crusts have the advantage that they grow on hard substrate in areas with strong bottom currents and low particle sedimentation. Hence, the recorded isotopic composition is not disturbed by detrital or diagenetic inputs but reflects solely the isotopic composition of seawater.

2. Study area, samples and methods

The Bauer Basin is situated on the Nazca plate between the extinct, or at least mostly deactivated, Galapagos Rise spreading center (GPR) to the east and the active EPR to the west (Fig. 1). Sediments from this basin, formerly called "Bauer Deep", are

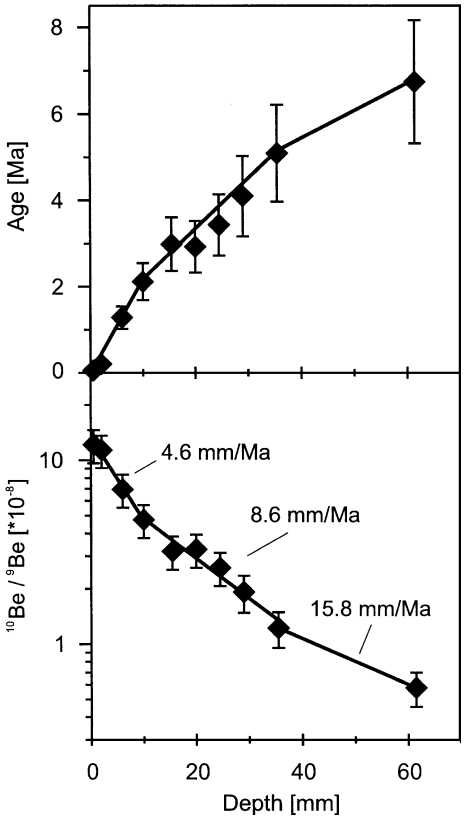

Fig. 2. Calculated age and ^{10}Be/^{9}Be versus depth for crust Yaloc. The calculated growth rates for the various depth intervals are labeled. Ages have been calculated with a half-life for ^{10}Be of 1.5 Myr and assuming a constant initial ^{10}Be/^{9}Be ratio.

rich in metals, especially Fe, Mn, Cu and Ni [31], and heat-flow patterns show a bimodal distribution characteristic of areas of hydrothermal circulation [32].

Crust D22-3 (hereafter called Yaloc) was recovered during cruise Yaloc 73 in a water depth of 4435–4214 m. The exact location (13°40.8′S, 102°08.1′W; Fig. 1) is ~500 km west of the GPR and ~1000 km east of the EPR. The oceanic basement in this area is about 20 million years old and is considered to have been produced mostly at the GPR [33]. Crust Yaloc is 68

Table 2
Pb isotope time-series for crust Yaloc (D22-3)

Depth interval (mm)	Age[a] (Ma)	$^{208}Pb/^{204}Pb$ ± 0.0075	$^{207}Pb/^{204}Pb$ ± 0.0025	$^{206}Pb/^{204}Pb$ ± 0.0020	$^{208}Pb/^{206}Pb$ ± 0.00024	$^{207}Pb/^{206}Pb$ ± 0.000060
0.5	0.109	38.4299	15.5876	18.5840	2.06786	0.838749
1.5	0.326	38.4430	15.5921	18.5866	2.06830	0.838886
2.5	0.543	38.4636	15.5965	18.5947	2.06852	0.838771
3.5	0.761	38.4306	15.5829	18.5954	2.06667	0.837997
4.5	0.978	38.4956	15.6010	18.6193	2.06752	0.837897
Duplicate	0.978	38.4959	15.6016	18.6199	2.06744	0.837901
5.5	1.196	38.4303	15.5888	18.5905	2.06720	0.838539
6.5	1.413	38.3751	15.5813	18.5576	2.06791	0.839623
7.5	1.630	38.2933	15.5649	18.5184	2.06783	0.840508
Duplicate	1.630	38.2963	15.5663	18.5194	2.06791	0.840538
8.5	1.848	38.2673	15.5616	18.5003	2.06849	0.841151
9.5	2.065	38.2354	15.5546	18.4860	2.06835	0.841425
10.5	2.232	38.2291	15.5533	18.4811	2.06857	0.841587
11.5	2.349	38.2364	15.5574	18.4769	2.06945	0.842014
12.5	2.466	38.2134	15.5512	18.4663	2.06937	0.842140
13.5	2.583	38.2288	15.5569	18.4687	2.06993	0.842342
14.5	2.700	38.2294	15.5572	18.4686	2.06997	0.842364
18	3.108	38.2298	15.5543	18.4778	2.06897	0.841785
22	3.576	38.2801	15.5653	18.4949	2.06983	0.841609
24	3.809	38.3156	15.5732	18.5040	2.07067	0.841614
26	4.043	38.3142	15.5690	18.5058	2.07040	0.841306
28	4.277	38.3364	15.5729	18.5194	2.07004	0.840895
30	4.510	38.3326	15.5736	18.5183	2.07001	0.840997
Duplicate	4.510	38.3253	15.5711	18.5163	2.06983	0.840941
32	4.744	38.2899	15.5655	18.5016	2.06955	0.841312
34	4.978	38.2589	15.5633	18.4847	2.06974	0.841947
36	5.185	38.2387	15.5630	18.4697	2.07039	0.842622
38	5.311	38.1978	15.5540	18.4501	2.07031	0.843034
40	5.438	38.1414	15.5413	18.4257	2.06993	0.843426
42	5.565	38.1636	15.5495	18.4276	2.07100	0.843815
46	5.819	38.1200	15.5431	18.3998	2.07176	0.844742
48	5.946	38.1244	15.5448	18.4018	2.07182	0.844745
50	6.072	38.0947	15.5396	18.3885	2.07168	0.845082
52	6.199	38.0860	15.5390	18.3838	2.07172	0.845251
54	6.326	38.0767	15.5373	18.3833	2.07122	0.845170
56	6.453	38.0096	15.5213	18.3655	2.06964	0.845143
58	6.580	38.0381	15.5294	18.3748	2.07016	0.845173
60	6.706	37.9982	15.5153	18.3691	2.06861	0.844626
62	6.833	38.0261	15.5224	18.3784	2.06903	0.844602
64	6.960	38.0654	15.5338	18.3906	2.06979	0.844669
66.5	7.119	38.0462	15.5268	18.3904	2.06881	0.844312

Errors for all Pb isotope ratios are reported as 2σ standard deviations resulting from repeated analysis of NIST SRM981 ($n=27$) in the course of the sample measurements. For better compatibility with previously published data, all ratios were normalized to the NIST NBS981 values of Galer and Abouchami [38].

[a] Ages were calculated using growth rates derived by $^{10}Be/^{9}Be$ ratios (Table 1, Fig. 2).

mm thick, its color is grayish–brownish with visible growth layers and its porosity is relatively high.

In order to date the crust by the $^{10}Be/^{9}Be$ technique, manual sampling of a depth profile was carried out perpendicular to the growth layers. Chemical preparation for the ^{10}Be AMS measurements closely followed the method described by Henken-Mellies et al. [34]. The ^{10}Be concentrations were measured at the Zürich AMS facility of the Paul Scherrer Institute and ETH Zürich, Switzerland. ^{9}Be concentrations were measured on the same aliquots at the Laboratory of Inorganic Chemistry, ETH Zürich, Switzerland using an ELAN DRC ICP-MS 6100 instrument. Further details about the applied methods can be found elsewhere [35].

Sampling for the Pb isotope profile was performed using a computer-controlled milling device to obtain continuous high-resolution time-series. Chemical separation closely followed the method described by Lugmair and Galer [36]. The Pb isotope ratios were measured with a Nu Plasma MC-ICP-MS at the ETH Zürich using a Tl-doping procedure to correct for instrumental mass bias [37]. Repeat analyses of the NIST SRM981 Pb standard gave an external reproducibility (2σ standard deviation) as reported in Table 2. However, Pb isotope data obtained for several ferromanganese crust measurement sessions over the period of 3 years (Nu Plasma MC-ICP-MS, ETH Zürich) indicate an external precision (2σ standard deviation) of 100–130 ppm for $^{206}Pb/^{204}Pb$, 100–160 ppm for $^{207}Pb/^{204}Pb$ and 100–200 ppm for $^{208}Pb/^{204}Pb$. All Pb isotope results were normalized to the Pb isotopic composition of NIST SRM981 given by Galer and Abouchami [38].

Neodymium and Hf isotope analyses were performed on the same aliquots. Due to larger samples required for Hf isotope measurements compared to Pb isotope measurements, two to four of the samples used for Pb isotope analyses had to be combined. The chemical separation of Hf followed the two-column procedure described by Lee et al. [39] and Nd separation chemistry was performed on the fluorides precipitated in the initial step of the Hf chemistry. After converting the solution to Cl^{-} form, separation and purification was carried out as described by Cohen et al. [40]. Neodymium and Hf isotope ratios were also measured with a Nu Plasma MC-ICP-MS at the ETH Zürich. To correct for instrumental mass bias, $^{176}Hf/^{177}Hf$ ratios were normalized to a $^{179}Hf/^{177}Hf$ ratio of 0.7325 and $^{143}Nd/^{144}Nd$ ratios were normalized to a $^{146}Nd/^{144}Nd$ ratio of 0.7219. Repeated analysis of the JMC475 Hf

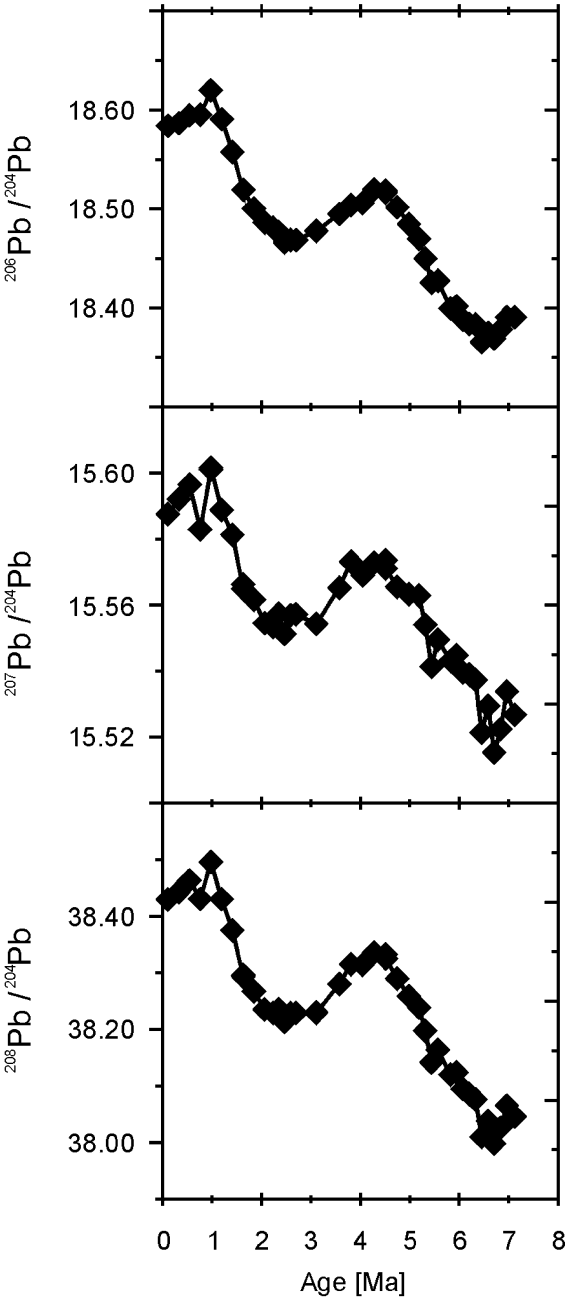

Fig. 3. Lead isotope time-series for crust Yaloc.

standard and the JMC Nd standard in the course of the sample measurements yielded an external precision of 0.51 ε units on $^{176}Hf/^{177}Hf$ (2σ standard deviation, $n=32$) and 0.20 ε units on $^{143}Nd/^{144}Nd$ (2σ standard deviation, $n=24$). For compatibility, all reported Hf isotope results were normalized to a $^{176}Hf/^{177}Hf$ ratio of 0.282160 for JMC475. All reported Nd isotope results were normalized to a nominal $^{143}Nd/^{144}Nd$ ratio of 0.511858 for La Jolla. For further analytical details, see Table 3 and van de Flierdt et al. [41].

3. Results

^{10}Be and ^{9}Be concentrations, $^{10}Be/^{9}Be$ ratios, and calculated growth rates for crust Yaloc are presented in Table 1 and $^{10}Be/^{9}Be$ data are plotted as a function of depth in Fig. 2. Assuming a constant initial $^{10}Be/^{9}Be$ ratio, a constant growth rate does not fit all $^{10}Be/^{9}Be$ data within error. The growth rates that give the best exponential fits are 4.6 mm/Myr for the uppermost 10 mm, 8.6 mm/Myr for 10–35.5 mm and 15.8 mm/Myr for the lower parts of the crust (35.5–61.5 mm). The $^{10}Be/^{9}Be$ record shows an apparent discontinuity at a depth of 15.5 and 20 mm, but since the error bars of both data points overlap with the exponential best fit this is not statistically significant (Fig. 2). The growth rates in the lower parts of the crust are significantly higher than typically observed in hydrogenetic ferromanganese crusts (1–6 mm/Myr; e.g. [42]) and are more consistent with those of mixed hydrogenetic-hydrothermal crusts.

To determine the origin of crust Yaloc (hydrothermal, hydrogenetic or diagenetic), concentrations of Fe, Mn, Co, Ni and Cu were analyzed at 11 depth intervals through the crust [43]. The results reveal no

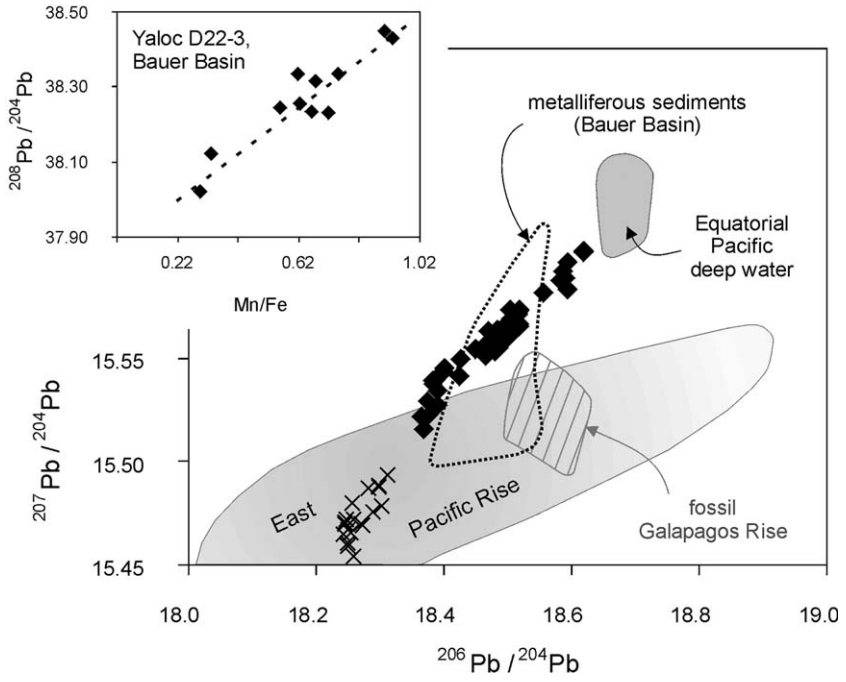

Fig. 4. Pb–Pb mixing plot for crust Yaloc. Data points for crust Yaloc are shown as black diamonds. Data source for the field of the East Pacific Rise: Petrological Database of the Ocean floor, PETDB, http://petdb.ldeo.columbia.edu/petdb/. Data source for the Equatorial Pacific deep water field: [44,45]. Crosses represent data from the EPR at 10°N, which are discussed in the text [62]. Dashed line defines the field for metalliferous sediments from the Bauer Basin [14,15,18] and hatched area corresponds to >15 Myr old basalts from the Galapagos Rise [14]. Inlet: Correlation of Mn/Fe ratios with $^{208}Pb/^{204}Pb$ ratios for crust Yaloc; $r^2=0.86$.

major deviations from the composition expected for hydrogenetic ferromanganese crusts for the uppermost 35.5 mm. Two samples analyzed from the older parts of the crust (>5 Myr) exhibit significant enrichments in Fe, Cu and a slight depletion in Co. A more complete set of elements (51) was determined for three crust layers (0–7, 7–29 and 29–64 mm) and shows a marked and continuous decrease from the surface layer to the basal layer in Co (1262–784 ppm) and the opposite trend in Cu (812–1497 ppm). Other elements show continuous but less pronounced decreases (Be, Ga, Pb and Sr) and increases (Li, Sb, Sn, Zn and Zr) with increasing depth in the crust (J.R. Hein, unpublished data). The Mn/Fe ratios of crust Yaloc are between 0.3 and 0.9, which according to Hein et al. [42] is typical for mixed hydrogenetic-hydrothermal crusts. Unambiguous hydrothermal overprint, however, is only visible in the lowermost part of the crust (>35.5 mm), indicated by Mn/Fe ratios lower than 0.5, a growth rate of 15.8 mm/Myr, depleted Co concentrations, enriched Cu concentrations and low (unradiogenic) Pb isotope ratios.

High resolution and high precision Pb isotopic compositions were determined for 38 samples of crust Yaloc (Table 2, Fig. 3). The Pb isotope ratios display strikingly similar patterns and show a large variation with a general upward trend from lower (less radiogenic) ratios in the past to higher (more radiogenic) values at present (Fig. 3). The overall range of the data is 18.37–18.62, 15.52–15.60 and 38.00–38.50, for $^{206}Pb/^{204}Pb$, $^{207}Pb/^{204}Pb$ and $^{208}Pb/^{204}Pb$, respectively. In more detail, a pronounced upward trend started at ~6.4 Ma and lasted until ~4.4 Ma. Then, the ratios decreased again and a second distinct upward shift is observed for the time-interval between ~2.9 and ~1 Ma.

In Pb–Pb isotope diagrams, our time-series data from crust Yaloc plot on a straight line reflecting the control of two predominant endmembers, which are identified as MORB represented by EPR data and

Table 3
Nd and Hf isotope time-series for crust Yaloc (D22-3)

Depth interval [mm]	Age* [Ma]	$^{176}Hf/^{177}Hf$[a] ± 2σ S.E.	ε_{Hf} (0)[b] ± 2σ S.D.	$^{143}Nd/^{144}Nd$[c] ± 2σ S.E.	ε_{Nd} (0)[d] ± 2σ S.D.
0–2	0.22	0.282954 ± 7	6.55 ± 0.51	0.512476 ± 9	−3.17 ± 0.20
Duplicate				0.512486 ± 12	−2.96 ± 0.24
5–6	1.20	0.282968 ± 8	7.03 ± 0.51	0.512483 ± 8	−3.02 ± 0.20
10–11	2.23	0.282957 ± 7	6.65 ± 0.51	0.512494 ± 7	−2.82 ± 0.20
Duplicate		0.282961 ± 7	6.78 ± 0.51		
15–17	2.88	0.282968 ± 7	7.04 ± 0.51	0.512499 ± 6	−2.71 ± 0.20
21–23	3.58	0.282959 ± 7	6.72 ± 0.51	0.512490 ± 6	−2.89 ± 0.20
27–29	4.28	0.282984 ± 7	7.62 ± 0.51	0.512490 ± 6	−2.89 ± 0.20
Duplicate		0.282956 ± 9	6.60 ± 0.51		
33–35	4.98	0.282956 ± 7	6.60 ± 0.51	0.512477 ± 6	−3.15 ± 0.20
39–41	5.44	0.282946 ± 6	6.27 ± 0.51	0.512473 ± 8	−3.21 ± 0.20
45–47	5.82	0.282947 ± 7	6.28 ± 0.51	0.512456 ± 7	−3.55 ± 0.20
Duplicate				0.512471 ± 6	−3.27 ± 0.20
51–53	6.20	0.282959 ± 6	6.74 ± 0.51	0.512465 ± 7	−3.37 ± 0.20
57–59	6.58	0.282936 ± 6	5.92 ± 0.51	0.512463 ± 6	−3.41 ± 0.20
Duplicate		0.282941 ± 7	6.08 ± 0.51		
65–68	7.12	0.282951 ± 9	6.42 ± 0.51	0.512463 ± 6	−3.41 ± 0.20

[a] For compatibility, all ratios were normalized to a JMC475 value of 0.282160; given errors represent 2σ standard errors of individual measurements; actually measured JMC475 values on 2 consecutive measuring days were 0.282175 ± 14 (2σ S.D.; $n=32$).

[b] Calculated with $^{176}Hf/^{177}Hf_{CHUR}$= 0.282769 [64]; errors for ε_{Hf} are reported as 2σ standard deviations resulting from repeated analysis of the JMC475 standard in the course of the sample measurements.

[c] For compatibility, all ratios were normalized to a nominal La Jolla value of 0.511858; for further details, see van de Flierdt et al. [41]; given errors represent 2σ standard errors of individual measurements; actually measured JMC values on two consecutive measuring days were 0.511813 ± 10 (2σ S.D.; $n=24$).

[d] Calculated with $^{143}Nd/^{144}Nd_{CHUR}=0.512638$; errors for ε_{Nd} are reported as 2σ standard deviations resulting from repeated analysis of the JMC Nd standard in the course of the sample measurements; in one case where the internal error is larger than the external one (duplicate), the internal error is reported.

* Ages were calculated using growth rates derived by $^{10}Be/^{9}Be$ ratios (Table 1, Fig. 2).

Equatorial Pacific deep water as obtained from data for hydrogenetic Equatorial Pacific crusts [44,45] (Fig. 4). The surface values of Yaloc are only slightly lower than those of Equatorial Pacific crust surfaces and the Pb isotopic composition at 7.1 Ma is identical to that of MORB from the EPR (for a compilation of data, see the Petrological Database of the Ocean floor, PETDB, http://petdb.ldeo.columbia.edu/petdb/). Moreover, the Pb isotopes show a pronounced covariance with Mn/Fe ratios as displayed for the $^{208}Pb/^{204}Pb$ ratios in Fig. 4, pointing again towards the same two predominant endmembers controlling the Pb isotope evolution of crust Yaloc. Most of the Pb data, except for the youngest and oldest samples, overlap with the field of metalliferous sediments from the Bauer Basin (Fig. 4; [14,15,18]). Data from Miocene basalts (>15 Ma) from the fossil GPR [14] plot in the field of EPR basalts, but do exhibit too high $^{206}Pb/^{204}Pb$ ratios to serve as an endmember for the Pb isotope ratios of crust Yaloc (Fig. 4).

Twelve samples of crust Yaloc have been analyzed for their Nd and Hf isotopic composition (Table 3, Fig. 5). Both isotope systems show very constant values over the past 7.1 Myr, exhibiting variations which hardly exceed the analytical error of the measurements. While Hf data scatter around an average value of $\varepsilon_{Hf} = 6.6 \pm 0.4$, the Nd data show a slight upward trend of 0.7 ε units for the time interval from 5.8 to 2.9 Ma. The average ε_{Nd} value is -3.1 ± 0.3. Both time-series exhibit an isotopic composition indistinguishable from Equatorial Pacific deep water over the past 7.1 Myr (Fig. 5; [44]). Neither Nd nor Hf isotopes are coupled to the large variations observed in the Pb isotope patterns (Figs. 3, 5 and 6).

4. Discussion

Lead isotopes in crust Yaloc from the Bauer Basin indicate a two-component mixture of hydrothermal (MORB-like) and seawater Pb over the past 7.1 Myr, with the latter having become stepwise more predominant towards present day (Figs. 3 and 4). The pattern of the Pb isotope time-series reveals varying contributions of hydrothermal Pb, which can be explained as a direct consequence of the history of decreasing hydrothermal activity of the now probably extinct Galapagos Rise, and the development of the active East Pacific Rise. Hence, Pb isotope time-series from ferromanganese crusts can obviously serve to reconstruct the hydrothermal history of specific areas of the world's deep ocean. However, other hydrothermal sources within the Bauer Basin and changes in deep water circulation patterns in the area have to be considered viable explanations for the observed temporal variations as well and will be discussed in the following. In addition, the controversial subject of hydrothermal Hf supply to the deep ocean can be addressed with the combined Hf–Nd–Pb dataset of crust Yaloc.

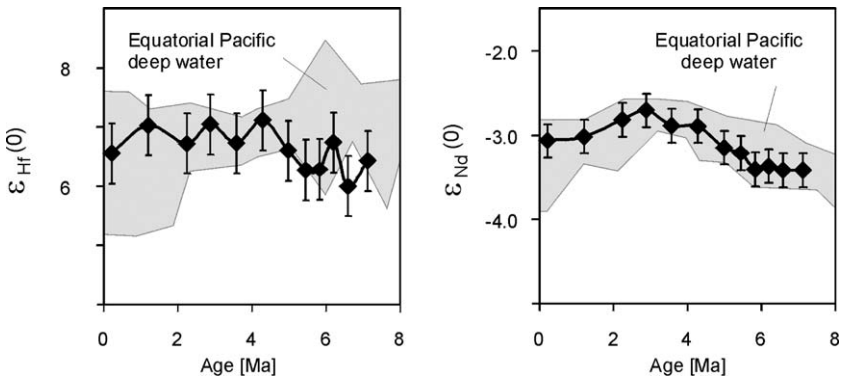

Fig. 5. Neodymium and Hf isotope time-series for crust Yaloc (eastern Equatorial Pacific) compared with Equatorial Pacific deep water time-series [39,44].

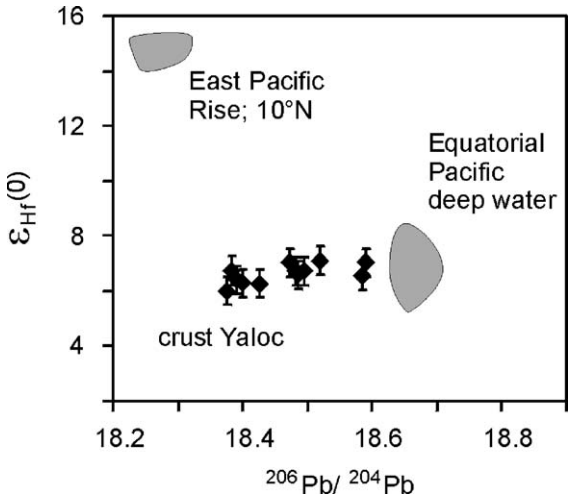

Fig. 6. $^{206}Pb/^{204}Pb$ ratios vs. ε_{Hf} of the time-series for crust Yaloc (eastern Equatorial Pacific) in comparison with Equatorial Pacific deep water time-series over the past 7 Myr [39,44] and basalts from the East Pacific Rise at 10°N [62]. No correlation of Pb and Hf isotopes can be observed for crust Yaloc. The mixture of hydrothermal fluids and seawater can explain Pb isotopes, whereas Hf isotopes in crust Yaloc have not recorded any hydrothermal imprint.

4.1. Evidence from Pb isotopes for hydrothermal activity

At the base of crust Yaloc (7.1 Ma) the Pb isotopic composition is similar to that of MORB indicating precipitation in the vicinity of hydrothermal vents (Fig. 4). This is supported by lowest Mn/Fe ratios (~ 0.3; Fig. 4) and highest growth rates (15.8 mm/Myr; Table 1, Fig. 2), which are indicative of hydrothermal origin (e.g. [42]). A progressive decrease of hydrothermal discharge to the Bauer Basin started at ~6.5 Ma and subsequently led to the observed change in the Pb isotope ratios towards more radiogenic values (Figs. 3 and 4), indicating increased proportions of seawater Pb. This upward trend ceased at ~ 4.4 Ma and from ~ 4.1 to ~ 2.9 Ma Pb isotopes became less radiogenic again suggesting another phase of enhanced hydrothermal contributions. Three possibilities exist for the source of hydrothermal Pb in the Bauer Basin: (i) advection to the east from the crest of the active East Pacific Rise, (ii) local hydrothermal activity in the Bauer Basin itself or (iii) emanations of hydrothermal fluids from the abandoned Galapagos Rise.

Considering advection of hydrothermal Pb from the EPR, Edmond et al. [2] showed that particulate matter, entrained in a hydrothermal plume, can be transported for thousands of kilometers before final deposition. This transport occurs via dispersion within prevailing ocean currents and was documented previously for Pb on the basis of the Pb isotope distribution in metalliferous sediments [16]. The modern deep water circulation pattern in the eastern Equatorial Pacific is shown schematically in Fig. 1 [46]. Equatorial Pacific deep water enters the Bauer Basin by channeling through several deep passages (transform fault intersects) in the East Pacific Rise between 3°S and 10°S. For Southern Ocean water, there are two main pathways, the first of which is a narrow, deep pathway along the Peru–Chile trench at the east Pacific margin, and the second is a broader sill between the Nazca and Sala-y-Gomez Ridges. A western source of deep water in the Bauer Basin today is evident from temperature, salinity and oxygen concentrations [46], and is corroborated by the Nd isotope time-series of crust Yaloc (Fig. 5). Neodymium is in general quantitatively removed from hydrothermal fluids at vent sites (e.g. [27,28]). Hence, any hydrothermally dispersed Fe and Mn oxyhydroxides will not carry a hydrothermal Nd signature but scavenge Nd from seawater and record the isotopic composition of ambient deep water. Neodymium isotopes in the Bauer Basin are identical to values for (central) Equatorial Pacific deep water and exhibit ratios that are nearly invariant over the past 7 Ma. The combined evidence from the Nd and Pb isotope evolutions precludes a major change in ocean circulation as the cause of the observed Pb isotope pattern. Moreover, it is unlikely that the majority of hydrothermal Pb observed at the location of crust Yaloc is advected from the EPR, since present day Pb isotopes indicate an approximately 30:70 mixture of hydrothermal Pb and seawater-derived Pb ($^{206}Pb/^{204}Pb$ = 18.25 and 18.71, respectively). This estimate is, however, only based on the isotopic compositions shown in Fig. 4. A two-component mixture with realistic concentrations for hydrothermal fluids and seawater ($[Pb]_{fluids}/[Pb]_{seawater}$ = 6000–90,000; [18,47,48]) and endmember isotopic compositions of $^{206}Pb/^{204}Pb$ = 18.25 and 18.71 and $^{207}Pb/^{204}Pb$ = 15.49 and 15.63 for MORB

and seawater, respectively, results in a present day contribution of hydrothermal fluids to seawater Pb of 0.004–0.00025%. This contribution was by a factor of 15 higher at 7 Ma (0.06–0.004%). We cannot, however, completely exclude the possibility that hydrothermal activity at the EPR in the sector between 3°S and 10°S was more important in the past in terms of plume export for the location of crust Yaloc than it is today.

4.2. History of the Galapagos Rise and the Bauer Basin

Our preferred interpretation relates the changes in the Pb isotope patterns of crust Yaloc to the activity of the now most likely extinct Galapagos Rise spreading center (Fig. 1). The main reason for this conclusion is the MORB-like Pb isotopic composition of the crust prior to 6.5 Ma and the pronounced upward shift afterwards. The timing coincides precisely with a proposed jump in spreading activity from the Galapagos Rise to the East Pacific Rise [49,50]. Note that the EPR field in Fig. 4 is used to represent the composition of the EPR and GPR due to the lack of data from the fossil GPR for the time-interval of interest. The only existing Pb isotope data from the fossil GPR were obtained from >15-Myr-old basalts from DSDP Site 319, drilled on the western flank of the extinct Galapagos Rise (Fig. 4; [14]). These data are, however, too radiogenic to serve as an endmember for crust Yaloc, pointing towards (i) a change in the isotopic composition of the source (GPR) with time or (ii) large heterogeneities in the composition of GPR lavas and fluids (K. Haase, personal communication) or (iii) an alternative source (EPR; see also Unruh and Tatsumoto [14]). Here, we assume that basalts (and fluids) from the ultimate activity of the GPR had similar Pb isotopic compositions to the EPR at the extension of the mixing line of crust Yaloc into the EPR field (Fig. 4).

The Galapagos Rise spreading center is an abandoned segment of the proto-EPR [49], extending from 5°S to 17°S and 95°W to 97°W ([51]; Fig. 1). Spreading at the GPR appears to have originated from the breakup of the Farallon plate into several smaller plates (e.g. Nazca plate and Cocos plate) around ~ 20 Ma. Active spreading probably started soon after this major plate reorganization (e.g. [33]). Near the end of the Miocene (~ 6.5 Ma), spreading on the GPR ceased, starting in the southern part and migrating northward. It was suggested that the EPR obtained its present configuration by several discrete westward jumps of the spreading center [33,49–52]. Fig. 7 shows a sketch map of this evolution as suggested by Rea [52,53] with three distinct jump events at 8.2 Ma (750 km), 6.5/6.4 Ma (850 km) and 5.7 Ma (650 km) at latitudes between 13.5°S and 4.5°S. On the basis of this, it has been proposed that, for a period of ~ 2 Myr, two spreading centers (EPR and GPR) were operating simultaneously, creating the so-called Bauer microplate. In contrast, Goff and Cochran [54] proposed an early existence of the Bauer microplate (soon after 20 Ma), and the existence of another spreading axis to the west of the GPR to account for the amount of lithosphere created between 20 and 8 Ma and for the geometry of the fracture zones.

Independent from details of the tectonic evolution of the Nazca plate prior to 8 Ma, it is evident from the Pb isotope data presented here that discharge of hydrothermally derived Pb did not abruptly end with the proposed jumps of spreading (Fig. 7). It is more likely that there was a progressive decrease in hydrothermal activity as indicated by the continuous upward trend in the Pb isotope patterns of crust Yaloc from ~ 6.5 to ~ 4.4 Ma. In addition, the Pb isotope record points to a renewed pulse of enhanced hydrothermal activity on the Galapagos Rise from 4.4 to 2.9 Ma (Fig. 3). This interpretation is supported by recent work that indicates that lavas were erupted at the GPR later than 6.5 Ma [55]. Moreover, based on local bathymetric and magnetic anomalies, McGuire and Hilde [56] suggested that ultra-slow spreading might have occurred until very recently (5–0 Ma). If true, there may have been associated hydrothermal activity at the GPR over the entire period of the past 6.5 Myr.

Another possibly source, which cannot be ruled out, is local hydrothermal activity in the Bauer Basin itself. According to Eakins et al. [57], the ancient Galapagos Rise revealed spreading rates of ~ 102 mm/year from 15 to 6 Ma. Since crust Yaloc shows a growth history of 7.1 Myr (Fig. 2), this implies that the location moved by ~ 60 km to the west in the time-interval from 7.1 to 6.5 Ma. This in turn would mean that already at 7.1 Ma the GPR was more than 400 km distant from the sampling site of crust Yaloc,

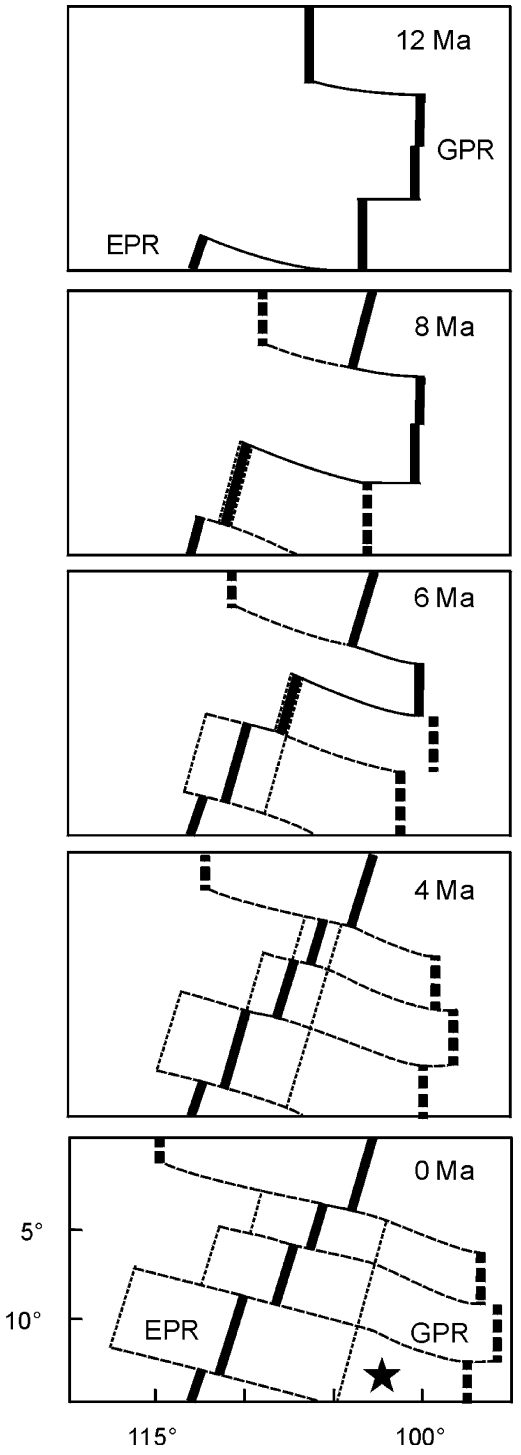

which at this point back in time exhibited a MORB-like Pb isotopic composition (Figs. 3 and 4). Therefore, the entire record, and especially the signal of renewed hydrothermal activity between 4.4 and 2.9 Ma, could be due to off-axis hydrothermal activity at adjacent locations in the Bauer Basin. This line of argumentation is supported by anomalously high heat flow data obtained by Anderson and Halunen [32], which is typical for hydrothermally active regions and is consistent with the Pb isotope time-series data for crust Yaloc.

4.3. In search of hydrothermal hafnium

The controversial issue whether hydrothermal Hf has played an important role for the dissolved Hf budget in the oceans (e.g. [29,30]) can be addressed by comparing the clearly hydrothermally influenced Pb isotope record of crust Yaloc with the Hf isotope record of the same profile (Fig. 6). If the deep water Hf isotopic composition at this location had been significantly affected by hydrothermal contributions, crust Yaloc should have recorded more radiogenic values in the past than at present, which is not observed. Hafnium isotopes are invariant within analytical error over the entire profile (Figs. 5 and 6).

To rule out that the lacking co-variance of Pb and Hf isotopes in crust Yaloc is due to the fact that the entire Hf isotope profile is hydrothermally overprinted, Hf isotope data should be compared with potential seawater and hydrothermal fluid endmembers as done for Pb isotopes (Fig. 4). However, no such data are available so far. For seawater, we can make the simplified assumption that the isotopic composition of hydrogenetic ferromanganese crusts is representative for ambient seawater. Such an assumption has been proved realistic for Nd isotopes (e.g. [58]). Furthermore, Nd and Hf isotopes in surface scrapings of ferromanganese crusts show coupling on a global scale, which means that a similar incorporation mechanism for Hf and Nd into crusts is feasible [59,60]. Following this approach, Equatorial

Fig. 7. Sketch map for the tectonic evolution and abandonment of Galapagos Rise spreading and initiation of spreading at each successive segment of the East Pacific Rise (modified after Rea [52]). The star marks the present location of crust Yaloc. EPR = East Pacific Rise, GPR = Galapagos Rise.

Pacific deep water exhibits ε_{Hf} values of 5.6–8.1 over the past 7 Myr (Fig. 6; [39]). Considering the hydrothermal fluid endmember, the Hf isotopic composition of basalts from the EPR can be regarded as a first order approximation. These basalts show ε_{Hf} values varying from 14 to 20 (for a compilation of data, see the Petrological Database of the Ocean floor, PETDB, http://petdb.ldeo.columbia.edu/petdb/). Moreover, MORB-like Hf isotope data ($\varepsilon_{Hf} > +10$) for marine ferromanganese precipitates have been obtained from hydrothermal manganese deposits, which formed below the sediment-seawater interface from the western Pacific volcanic arcs, the central Pacific Hawaiian hotspot ($\varepsilon_{Hf} \sim +13$; [30]), and from a hydrothermal manganese crust from the Lesser Antilles back-arc basin ($\varepsilon_{Hf} = +11$ to $+12$; Frank et al., in preparation). Hydrothermal deposits are generated by direct precipitation of metals from seawater-dominated hydrothermal fluids (e.g. [61]), and therefore suggest that Hf in the fluids has a mantle-like isotopic signature. All these data clearly suggest that the Hf from the entire Yaloc profile ($\varepsilon_{Hf} = 5.9–7.6$; Table 3, Fig. 5) is of seawater origin.

To further corroborate this conclusion, Fig. 6 shows the only available dataset for combined Pb and Hf isotopes from EPR basalts (location at 10°N; [62]). While Pb isotopes from these basalts could serve as hypothetical endmember for crust Yaloc (Fig. 4), the Hf isotopic composition ($\varepsilon_{Hf} = 14.2–15.1$; [62]) is much more radiogenic than observed from crust Yaloc ($\varepsilon_{Hf} = 6.6 \pm 0.4$) and a significant hydrothermal Hf contribution is hard to reconcile.

Supporting evidence is moreover coming from the coupling of Nd and Hf isotopes in crust Yaloc (Fig. 5). For Nd, it has been shown that the flux of hydrothermal Nd is negligible, because of very strong particulate scavenging of rare earth elements in and near vents [27,28]. Since the Nd isotope profile of crust Yaloc exhibits values indistinguishable from Equatorial Pacific deep water (Fig. 5), it is likely that crust Yaloc grew from this water mass and recorded its isotopic composition, without being disturbed by potential terrigenous sources (see Section 4.1). Hence, the observed Hf isotope signature, which is also indistinguishable from Equatorial Pacific deep water (Fig. 5), supports once more the lack of a hydrothermal Hf component in crust Yaloc. This conclusion is validated by data from other mixed hydrogenetic-hydrothermal crusts, which seem to loose their hydrothermal ε_{Hf} signal almost immediately (within tens of meters or less) as evidenced by the Gulf of California crust analyzed by Godfrey et al. [30].

In summary, the data presented here for the mixed hydrogenetic-hydrothermal crust Yaloc strongly suggest that hydrothermal Hf does not travel far from hydrothermal vent sites, if at all, and is therefore insignificant for the global marine Hf budget.

5. Concluding remarks

MORB-like Pb isotopic compositions in crust Yaloc (Bauer Basin, eastern Equatorial Pacific) reveal clear evidence for hydrothermal supply of metals proximal to the location where the crust formed at 7 Ma. This is attributed to hydrothermal activity at the now at least nearly extinct Galapagos Rise. The evolution of the Pb isotopic composition towards more radiogenic, seawater-like values from 6.5 Ma onwards, indicates stepwise decreasing hydrothermal contributions, rather than an abrupt end of the hydrothermal activity. This is interpreted as a consequence of the proposed westward shift in spreading from the Galapagos Rise to the East Pacific Rise at ~6.5 Ma. Besides this major shift in spreading, a second, previously unrecognized, hydrothermal event was recorded by the Pb isotopes, which could either be due to off-axis hydrothermal activity in the Bauer Basin or due to a pulse of hydrothermal Pb derived from the still active or reactivated Galapagos Rise (4.4–2.9 Ma). With our present knowledge of the development of the Galapagos Rise, we can exclude neither of these. In order to gain better constraints on the history of hydrothermal contributions in the Bauer Basin, a detailed investigation of Pb isotope time-series from ferromanganese crusts or sediments from both sides of the Galapagos Rise and within the Bauer Basin would be needed. The application of Pb isotope time-series in ferromanganese crusts looks like a promising tool to trace the variability of hydrothermal activity on a regional scale over time.

In contrast, Hf isotopes exhibit typical seawater values in the same crust and the Yaloc record thus provides strong evidence against any significant contribution of hydrothermal Hf to the seawater Hf budget.

It is more likely that hydrothermal Hf is precipitated directly at active vent sites analogous to Nd.

Acknowledgements

H. Baur, M. Meier, U. Menet, D. Niederer, F. Oberli, B. Rütsche and A. Süsli are gratefully acknowledged for providing assistance with technical problems. M. Rehkämper, C. Stirling, H. Williams and S. Woodland is thanked for keeping the machines running smoothly. We thank Oregon State University for a split of crust Yaloc and K. Haase for discussion. W. Abouchami and two anonymous reviewers are acknowledged for their comments and suggestions. This research was funded by the Schweizerische Nationalfonds (SNF). ***[BARD]***

References

[1] J.B. Corliss, J. Dymond, L.I. Gordon, J.M. Edmond, R.P. Von Herzen, R.D. Ballard, K. Green, D. Williams, A. Bainbridge, K. Crane, T.J.H. Van Andel, Exploration of submarine thermal springs on the Galapagos Rift, Science 203 (1979) 1073–1083.

[2] J.M. Edmond, K.L. Von Damm, R.E. McDuff, C.I. Measures, Chemistry of hot springs on the East Pacific Rise and their effluent dispersal, Nature 297 (1982) 187–191.

[3] K.L. von Damm, Seafloor hydrothermal activity: black smoker chemistry and chimneys, Annu. Rev. Earth Planet. Sci. 18 (1990) 173–204.

[4] H. Elderfield, A. Schultz, Mid-ocean ridge hydrothermal fluxes and the chemical composition of the ocean, Annu. Rev. Earth Planet. Sci. 24 (1996) 191–224.

[5] M.D. Rudnicki, H. Elderfield, A chemical model of the buoyant and neutrally buoyant plume above the TAG vent field, 26 degrees N, Mid-Atlantic Ridge, Geochim. Cosmochim. Acta 57 (1993) 2939–2957.

[6] R.A. Mills, H. Elderfield, J. Thomson, A dual origin for the hydrothermal component in a metalliferous sediment core from the Mid-Atlantic Ridge, J. Geophys. Res. 98 (1993) 9671–9681.

[7] C.R. German, A.C. Campbell, J.M. Edmond, Hydrothermal scavenging at the Mid-Atlantic Ridge: modification of trace element dissolved fluxes, Earth Planet. Sci. Lett. 107 (1991) 101–114.

[8] J.E. Lupton, H. Craig, A major helium-3 source at 15°S on the East Pacific rise, Science 214 (1981) 13–18.

[9] R.A. Mills, H. Elderfield, Hydrothermal activity and the geochemistry of metalliferous sediment, in: S.E. Humphris, R.A. Zierenberg, L.S. Mullineaux, R.E. Thomson (Eds.), Hydrothermal Systems—Physical, Chemical, Biological, and Geological Interactions, Geophysical Monograph, vol. 91, American Geophysical Union, Washington, DC, 1995, pp. 392–407.

[10] M.-H. Cormier, W.B.F. Ryan, A.K. Shah, W. Jin, A.M. Bradley, D.R. Yoerger, Waxing and waning volcanism along the East Pacific Rise on a millennium time scale, Geology 31 (2003) 633–636.

[11] G.L. Früh-Green, D.S. Kelley, S.M. Bernasconi, J.A. Karson, K.A. Ludwig, D.A. Butterfield, C. Boschi, G. Proskurowski, 30,000 years of hydrothermal activity at the lost city vent field, Science 301 (2003) 495–498.

[12] K. Bostrom, M.N.A. Peterson, O. Joensuu, D.E. Fisher, Aluminium-poor ferromanganoan sediments on active ocean ridges, J. Geophys. Res. 74 (1969) 3261–3270.

[13] V. Marchig, Hydrothermal activity on the southern, ultrafast-spreading segment of the East Pacific Rise, in: D.S. Cronan (Ed.), Handbook of Marine Mineral Deposits, CRC Press, Boca Raton, 2000, pp. 309–325.

[14] D.M. Unruh, M. Tatsumoto, Lead isotopic composition and uranium, thorium, and lead concentrations in sediments and basalts from the Nazca plate, in: R.S. Yeats, S.R. Hart, et al. (Eds.), Init. Rpts. DSDP, vol. 34. U.S. Governmental Printing Office, Washington, 1976, pp. 341–347.

[15] E.J. Dasch, Lead isotopic composition of metalliferous sediments from the Nazca plate, Geol. Soc. Am., Mem. 154 (1981) 199–209.

[16] T.J. Barrett, P.N. Taylor, J. Lugowski, Metalliferous sediments from DSDP Leg 92: the East Pacific Rise transect, Geochim. Cosmochim. Acta 51 (1987) 2241–2253.

[17] L.V. Godfrey, R. Mills, H. Elderfield, E. Gurvich, Lead behaviour at the TAG hydrothermal vent field, 26°N, Mid-Atlantic Ridge, Mar. Chem. 46 (1994) 237–254.

[18] B. Peucker-Ehrenbrink, A.W. Hofmann, S.R. Hart, Hydrothermal lead transfer from mantle to continental crust: the role of metalliferous sediments, Earth Planet. Sci. Lett. 125 (1994) 129–142.

[19] E.J. Dasch, J.R. Dymond, G.R. Heath, Isotopic analysis of metalliferous sediment from the East Pacific Rise, Earth Planet. Sci. Lett. 13 (1971) 175–180.

[20] T.J. Barrett, H. Friedrichsen, Elemental and isotopic compositions of some metalliferous and pelagic sediments from the Galapagos mounds area, DSDP Leg 70, Chem. Geol. 36 (1982) 275–298.

[21] J.H. Chen, G.J. Wasserburg, The U–Th–Pb systematics in hot springs on the East Pacific Rise at 21°N and Guaymas basin, Geochim. Cosmochim. Acta 50 (1986) 2467–2479.

[22] H. Craig, S. Krishnaswami, B.L.K. Somayajulu, ^{210}Pb–^{226}Ra: radioactive disequilibrium in the deep sea, Earth Planet. Sci. Lett. 17 (1973) 295–305.

[23] B.K. Schaule, C.C. Patterson, Lead concentrations in the northeast Pacific: evidence for global anthropogenic perturbations, Earth Planet. Sci. Lett. 54 (1981) 97–116.

[24] J.K. Cochran, T. McKibbin-Vaughan, M.M. Dornblaser, D. Hirschberg, H.D. Livingston, K.O. Buesseler, ^{210}Pb scavenging in the North Atlantic and North Pacific Oceans, Earth Planet. Sci. Lett. 97 (1990) 332–352.

[25] I. Vlastélic, W. Abouchami, S.J.G. Galer, A.W. Hofmann, Geographic control on Pb isotope distribution and sources in Indian Ocean Fe–Mn deposits, Geochim. Cosmochim. Acta 65 (2001) 4303–4319.
[26] R.A. Mills, D.M. Wells, S. Roberts, Genesis of ferromanganese crusts from the TAG hydrothermal field, Chem. Geol. 176 (2001) 283–293.
[27] A.N. Halliday, J.P. Davidson, P. Holden, R.M. Owen, A.M. Olivarez, Metalliferous sediments and the scavenging residence time of Nd near hydrothermal vents, Geophys. Res. Lett. 19 (1992) 761–764.
[28] C.R. German, G.P. Klinkhammer, J.M. Edmond, A. Mitra, H. Elderfield, Hydrothermal scavenging of rare-earth elements in the ocean, Nature 345 (1990) 516–518.
[29] W.M. White, J. Patchett, D. Ben Othman, Hf isotope ratios of marine sediments and Mn nodules: evidence for a mantle source of Hf in seawater, Earth Planet. Sci. Lett. 79 (1986) 46–54.
[30] L.V. Godfrey, D.-C. Lee, W.F. Sangrey, A.N. Halliday, V.J.M. Salters, J.R. Hein, W.M. White, The Hf isotopic composition of ferromanganese nodules and crusts and hydrothermal manganese deposits: implications for seawater Hf, Earth Planet. Sci. Lett. 151 (1997) 91–105.
[31] G.M. McMurtry, W.C. Burnett, Hydrothermal metallogenesis in the Bauer Deep of the south-eastern Pacific, Nature 254 (1975) 42–44.
[32] R.N. Anderson, J.J. Halunen, Implications of heat flow for metallogenesis in the Bauer Deep, Nature 251 (1974) 473–475.
[33] J. Mammerickx, E. Herron, L. Dorman, Evidence for two fossil spreading ridges in the southeast Pacific, Geol. Soc. Amer. Bull. 91 (1980) 263–271.
[34] W.U. Henken-Mellies, J. Beer, F. Heller, K.J. Hsü, C. Shen, G. Bonani, H.J. Hofmann, M. Suter, W. Wölfli, ^{10}Be and ^{9}Be in South Atlantic DSDP site 519: relation to geomagnetic reversals and to sediment composition, Earth Planet. Sci. Lett. 98 (1990) 267–276.
[35] T. van de Flierdt, M. Frank, A.N. Halliday, J.R. Hein, B. Hattendorf, D. Günther, P.W. Kubik, Lead isotopes in North Pacific deep water—implications for past changes in input sources and circulation patterns, Earth Planet. Sci. Lett. 209 (2003) 149–164.
[36] G.W. Lugmair, S.J.G. Galer, Age and isotopic relationships among the angrites Lewis Cliff 86010 and Angra dos Reis, Geochim. Cosmochim. Acta 56 (1992) 1673–1694.
[37] A.J. Walder, I. Platzner, P.A. Freedman, Isotope ratios measurement of lead, neodymium and neodymium–samarium mixtures, hafnium and hafnium–lutetium mixtures with a double focussing multiple collector inductively coupled plasma mass spectrometer, J. Anal. At. Spectrom. 8 (1993) 19–23.
[38] S.J.G. Galer, W. Abouchami, Practical application of lead triple spiking for correction of instrumental mass discrimination, Mineral. Mag. 62A (1998) 491–492.
[39] D.-C. Lee, A.N. Halliday, J.R. Hein, K.W. Burton, J.N. Christensen, D. Günther, Hafnium isotope stratigraphy of ferromanganese crusts, Science 285 (1999) 1052–1054.
[40] A.S. Cohen, R.K. O'Nions, R. Siegenthaler, W.L. Griffin, Chronology of the pressure–temperature history recorded by a granulite terrain, Contrib. Mineral. Petrol. 98 (1988) 303–311.
[41] T. van de Flierdt, M. Frank, D.-C. Lee, A.N. Halliday, B.C. Reynolds, J.R. Hein, New constraints on the sources and behavior of neodymium and hafnium in seawater from Pacific Ocean ferromanganese crusts, submitted to Geochim. Cosmochim. Acta. (in press).
[42] J.R. Hein, A. Koschinsky, M. Bau, F.T. Manheim, J.-K. Kang, L. Roberts, Cobalt-rich ferromanganese crusts in the Pacific, in: D.S. Cronan (Ed.), Handbook of Marine Mineral Deposits, CRC Press, Boca Raton, 2000, pp. 239–279.
[43] T. van de Flierdt, The Nd, Hf, and Pb isotopic composition of ferromanganese crusts and their paleoceanographic implications, PhD thesis, ETH Zürich, 2003.
[44] H.F. Ling, K.W. Burton, R.K. O'Nions, B.S. Kamber, F. von Blanckenburg, A.J. Gibb, J.R. Hein, Evolution of Nd and Pb isotopes in Central Pacific seawater from ferromanganese crusts, Earth Planet. Sci. Lett. 146 (1997) 1–12.
[45] T. van de Flierdt, M. Frank, A.N. Halliday, J.R. Hein, B. Hattendorf, D. Günther, P.W. Kubik, Deep- and bottom-water export from the Southern Ocean to the Pacific over the past 38 million years, Paleoceanography (2004) (doi:10.1029/2003PA000923).
[46] P. Lonsdale, Abyssal circulation of the Southeastern Pacific and some geological implications, J. Geophys. Res. 81 (1976) 1163–1176.
[47] J.H. Chen, U, Th, and Pb isotopes in hot springs on the Juan de Fuca Ridge, J. Geophys. Res. 92 (1987) 11411–11415.
[48] G. Ravizza, G.M. McMurtry, Osmium isotopic variations in metalliferous sediments from the East Pacific Rise and the Bauer Basin, Geochim. Cosmochim. Acta 57 (1993) 4301–4310.
[49] E.M. Herron, Sea-floor spreading and the Cenozoic history of East-Central Pacific, Geol. Soc. Am. Bull. 83 (1972) 1671–1692.
[50] R.N. Anderson, J.G. Sclater, Topography and evolution of the East Pacific Rise between 5°S and 20°S, Earth Planet. Sci. Lett. 14 (1972) 433–441.
[51] C.L. Mayes, L.A. Lawver, D.T. Sandwell, Tectonic history and new isochron chart of the South Pacific, J. Geophys. Res. 95 (1990) 8543–8567.
[52] D.K. Rea, Tectonics of the Nazca–Pacific divergent plate boundary, Geol. Soc. Am. Mem. 154 (1981) 27–61.
[53] D.K. Rea, Evolution of the East Pacific Rise between 3°S and 13°S since the middle Miocene, Geophys. Res. Lett. 5 (1978) 561–564.
[54] J.A. Goff, J.R. Cochran, The Bauer Scarp ridge jump: a complex tectonic sequence revealed in satellite altimetry, Earth Planet. Sci. Lett. 141 (1996) 21–33.
[55] K.M. Haase, N.A. Stroncik, Volcanism on the fossil Galapagos Rise spreading centre, SE Pacific, Fall Meeting, Suppl., EOS Trans. AGU, 83 (47), (2002) Abstract V52A-1278.
[56] J.C. McGuire, T.W.C. Hilde, Galapagos Rise to East Pacific Rise spreading history, Fall Meeting, Suppl., EOS Trans. AGU, 83 (47), (2002) Abstract T12D-1348.
[57] B.W. Eakins, P.F. Lonsdale, K.W. Skinner, New insights on

the history of the Bauer microplate and Galapagos Rise, Fall Meeting, Suppl., EOS Trans. AGU, 78 (46) (1997) Abstract T52B-10.

[58] D.J. Piepgras, G.J. Wasserburg, E.J. Dasch, The isotopic composition of Nd in different ocean masses, Earth Planet. Sci. Lett. 45 (1979) 223–236.

[59] F. Albarède, A. Simonetti, J.D. Vervoort, J. Blichert-Toft, W. Abouchami, A Hf–Nd isotopic correlation in ferromanganese nodules, Geophys. Res. Lett. 25 (1998) 3895–3898.

[60] K. David, M. Frank, R.K. O'Nions, N.S. Belshaw, J.W. Arden, J.R. Hein, The Hf isotope composition of global seawater and the evolution of Hf isotopes in the deep Pacific Ocean from Fe–Mn crusts, Chem. Geol. 178 (2001) 23–42.

[61] J.R. Hein, A. Koschinsky, P. Halbach, F.T. Manheim, M. Bau, J.-K. Kang, N. Lubick, Iron and manganese oxide mineralization in the Pacific, in: K. Nicholson, J.R. Hein, B. Bühn, S. Dasgupta (Eds.), Manganese Mineralization: Geochemistry and Mineralogy of Terrestrial Marine Deposits, Geol. Soc. London. Spec. Publ. 119 (1997) 123–138.

[62] K.W.W. Sims, S.J. Goldstein, J. Blichert-Toft, M.R. Perfit, P. Kelemen, D.J. Fornari, P. Michael, M.T. Murrell, S.R. Hart, D.J. DePaolo, G. Layne, L. Ball, M. Jull, J. Bender, Chemical and isotopic constraints on the generation and transport of magma beneath the East Pacific Rise, Geochim. Cosmochim. Acta 66 (2002) 3481–3504.

[63] M.D. Axelsson, I. Rodushkin, J. Ingri, B. Öhlander, Multielemental analysis of Mn–Fe nodules by ICP-MS: optimisation of analytical method, Analyst 127 (2002) 76–82.

[64] G.M. Nowell, P.D. Kempton, S.R. Noble, J.G. Fitton, A.D. Saunders, J.J. Mahoney, R.N. Taylor, High precision Hf isotope measurements of MORB and OIB by thermal ionisation mass spectrometry: insights into the depleted mantle, Chem. Geol. 149 (1998) 211–233.